ARTICLE   OPEN

Check for updates

Local symmetry distortion induced anomalous thermal conduction in thermoelectric layered oxyselenides

Bin Wei [1,2], Jiale Li[1], Yueyang Yang[2], Wang Li[1], Zhifang Zhou[2], Yunpeng Zheng[2], Wenyu Zhang[2], Yifan Chai[3], Zheng Chang[4], Ce-Wen Nan [2] and Yuan-Hua Lin[2 ✉]

Polyhedral distortion, associated closely with the atomic arrangement and interatomic interactions, drives many unique behaviors in solids, such as phase transition and negative thermal expansion. In thermoelectric heteroanionic oxides, the anionic polyhedra are widely present, but their effect on thermal transport is rarely investigated. Here, we report an anomalous thermal conduction induced by local symmetry distortion in layered oxyselenides via solving the Boltzmann transport equation based on first-principles calculations. We found interestingly that lighter BiCuSeO exhibits lower thermal conductivity than heavier BiAgSeO. Due to the different distorted degrees of CuSe4 and AgSe4 tetrahedrons, Cu prefers the in-plane vibration, while Ag has more tendency of out-of-plane vibration. Thus, the heat-carrying phonons dominated by the rattling-like vibration of Cu are significantly suppressed, resulting in lower thermal conductivity of BiCuSeO. This study highlights the importance of polyhedral distortion in regulating thermal conduction in layered heteroanionic materials.

INTRODUCTION

In thermoelectric materials, the heat-to-electricity conversion efficiency is directly determined by the figure of merit, $ZT = S^2\sigma T/\kappa$, where S, σ, T, and κ are the Seebeck coefficient, electrical conductivity, absolute temperature, and total thermal conductivity (including the electrical and lattice parts). As we all know, the parameters in ZT always couple with each other, making it difficult to improve the thermoelectric performance[1]. Searching for materials with low thermal conductivity to efficiently suppress heat conduction is thus crucial for thermoelectric applications. Layered oxides such as Na_xCoO_2 and $Ca_3Co_4O_9$, possessing advantages such as thermodynamical and chemical stability, environmental friendliness, and eco-friendliness, overcome the drawbacks of high thermal conductivity and low carrier mobility of traditional oxides, making them promising candidates for mid- to high- temperature thermoelectric applications[2]. With the natural superlattice structure, layered oxyselenides, such as BiCuSeO, Bi_2O_2Se, and newly reported $Bi_2LnO_4Cu_2Se_2$ (Ln is lanthanide), have attracted extensive attentions as thermoelectric materials due to the easily tunable thermal and electrical transport properties, especially the thermal conductivity, which can be reduced by orders of magnitude[2–6]. As shown in Supplementary Fig. 1a, it is obvious that layered oxyselenides hold extremely low thermal conductivity, compared to other oxides. Therefore, it is interesting to investigate the microscopic mechanism for the highly tunable thermal conductivity in the pristine system.

Among the family of layered oxyselenides, bismuth copper oxychalcogenides have been the focus of interest, mainly attributed to their unique electrical properties and ultralow thermal conductivity[7–9], compared to lanthanum oxychalcogenides[10,11] and Bi_2O_2Se[12,13]. For pristine BiCuSeO, the thermal conductivity at room temperature varies roughly from ~0.5 to ~1 W m^{-1} K^{-1} due to the different preparation techniques[14–19].

Recently, BiAgSeO has been successfully synthesized and has become a member of the oxyselenide thermoelectric family[20]. A low thermal conductivity of ~0.7 W m^{-1} K^{-1} (corrected for diffusivity and density[21]) has been reported experimentally, and the thermal transport mechanism has been discussed theoretically compared to BiCuSeO. The measured thermal conductivity is known to be affected by sample, synthesis, and measurement techniques. Therefore, as the diversity of the measured thermal conductivity of BiCuSeO, it is not rigorous to compare the value between these two systems.

BiAgSeO contains the heavier Ag atom (Cu: 63.55 versus Ag: 107.87) and weaker Ag-Se bond (predicted by the electronegativity difference[22]) and crystallizes into a layered structure similar to BiCuSeO (P4/*nmm* space group) where the $(Bi_2O_2)^{2+}$ layers are alternately stacked with the $(Ag_2Se_2)^{2-}$ tetragonal layers along *c*-axis (Supplementary Fig. 1b, c). Based on Slack's theory[23], a lower thermal conductivity is intuitively expected in BiAgSeO, which is explained by the calculation in ref. [20]. However, it is noted that the thermal transport calculation there does not converge by considering only the third-neighbor interactions in small super-cells compared to the previous calculation of BiCuSeO[24,25], i.e., the anharmonic effect is underestimated and the harmonic effect dominates, leading to a higher value of thermal conductivity of ~1.7 times than previous calculations[24,25]. Moreover, the calculated thermal conductivities in ref. [20]. also show large discrepancies between the measurement of BiAgSeO and the selected result of BiCuSeO, which is significantly inappropriate for evaluating the intrinsic property of thermoelectric materials. In addition, the fitted thermal conductivity of these two systems is comparable (~ 0.6 W m^{-1} K^{-1}) by using the Cahill model[26,27], indicating that other mechanisms beyond the Debye approximation dominate.

[1]Henan Key Laboratory of Materials on Deep-Earth Engineering, School of Materials Science and Engineering, Henan Polytechnic University, Jiaozuo 454000, PR China. [2]State Key Laboratory of New Ceramics and Fine Processing School of Materials Science and Engineering, Tsinghua University, Beijing 100084, PR China. [3]School of Materials and Metallurgy, Inner Mongolia University of Science and Technology, Baotou 014010, PR China. [4]School of Naval Architecture and Maritime, Zhejiang Ocean University, Zhoushan 316022, PR China. ✉email: linyh@tsinghua.edu.cn

In this work, we have systematically investigated the thermal and electrical transport behavior in layered BiCuSeO and BiAgSeO by solving the Boltzmann transport equation based on first-principles calculations. Interestingly, the thermal conductivity of BiCuSeO is lower than that of BiAgSeO, although the elastic modulus shows a conventional opposite result. Such anomaly is mainly induced by the local symmetry distortion of the irregular tetrahedron containing weakly bonded Cu (Ag)-Se, where the bonding configuration enforces Cu to be inclined to vibrate along the in-plane direction and yet Ag along the out-of-plane direction. The rattling-like Cu maintains a large third-order interatomic force constant (IFC) and induces the localized phonons along the in-plane direction, leading to ultralow group velocities and a short lifetime corresponding to the Cu-Se layer. This behavior is significantly powerful to reduce the thermal conductivity in layered materials because the thermal conductivity from the out-of-plane direction is originally low. The study unveils the critical role of polyhedral distortion in layered oxyselenides for regulating thermal and electrical transport.

RESULTS AND DISCUSSION
Thermal conductivity and phonon transport

In most semiconductors, thermal conductivity is generally dominated by phonons, which is also the case in bismuth copper oxychalcogenides[14–19]. Here, the lattice thermal conductivity is only considered (hereinafter referred to as thermal conductivity). Figure 1a shows the average thermal conductivity (calculated from the anisotropic value in Supplementary Fig. 2a). Our result of BiCuSeO shows good agreement with previous calculations because the calculation is fully converged[24,25]. As shown in Supplementary Fig. 2b, the converged value using eight-nearest neighbor interactions (cutoff distance is 5.36 Å) with

$3 \times 3 \times 2$ supercells for third-order force constant calculation is 60% of that using third-nearest neighbor interactions with $2 \times 2 \times 1$ supercells in ref. [20]. (details are shown in METHODS section). This result is more reasonable for analyzing the intrinsic thermal transport because the anharmonic effect is fully considered until the value converges with respect to the neighbor interactions and is in agreement with previous measurements (Fig. 1a and Supplementary Figure 2c)[15,20], while the calculation in ref. [20]. is higher than most of the previous measurements. Surprisingly, the thermal conductivities by relaxation time approximation (RTA) and exact numerical solutions of the Boltzmann equation (iterative) are both lower in BiCuSeO, contrary to the trend in ref. [20]. and unexpected based on the typical Slack's theory. The discrepancy between the RTA and iterative results indicates that Umklapp scattering is dominant for the thermal resistance. It should be noted that it is specious to simply compare the value between the calculation and experiment because the sample used for the measurement is not a perfect single crystal but a ceramic, in which the scattering mechanism is more complex. For example, although the phonon-defect, phonon-precipitate, and phonon-boundary scattering are taken into account, the calculation is still could not show a good agreement with measurement[15]. Therefore, investigation of pure phonon transport is more reliable to clarify why the thermal conductivity in BiCuSeO is lower than BiAgSeO intrinsically. Figure 1b shows the normalized cumulative thermal conductivity along the a-axis (in-plane). Phonons below 20 meV have a lower contribution in BiCuSeO (60%) than in BiAgSeO (76%), while phonons below 10 meV contribute ~90% to the thermal conductivity along the c-axis (out-of-plane) in both systems due to the weak interlayer interactions (Supplementary Fig. 2d). Such anisotropy well reflects the nature of the layered structure of both systems, and indicates
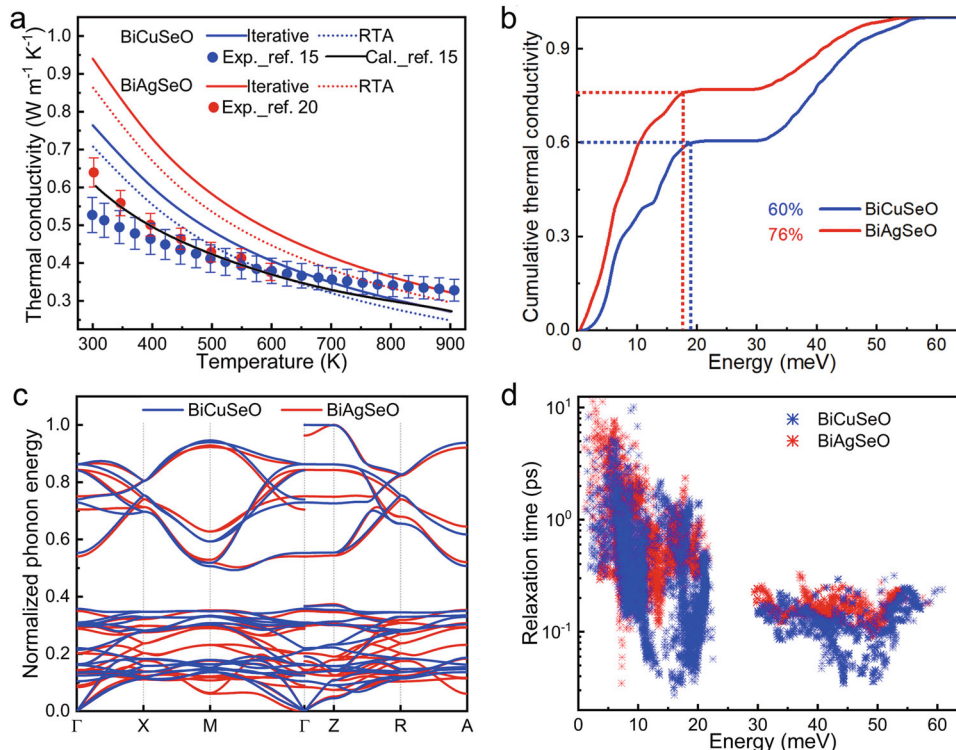

Fig. 1 Calculated phonon transport properties of BiCuSeO and BiAgSeO. a Temperature-dependent average thermal conductivity, compared to previous measurement[15,20]. RTA stands for the relaxation time approximation. Vertical lines are the absolute error obtained by the measurement with the uncertainty of 10% for BiCuSeO[15] and the diffusivity uncertainty of 5% for BiAgSeO[20] (the density uncertainty was corrected). **b** Normalized cumulative thermal conductivity along the a-axis. (**c**, **d**) are the comparison of the normalized phonon dispersion and the relaxation time, respectively.

that the transport difference is almost caused by the in-plane phonons located below 20 meV.

Figure 1c shows the comparison of the calculated phonon dispersion of BiCuSeO and BiAgSeO, which is renormalized from the exact phonon dispersion of Supplementary Fig. 3. It is found that the highly dispersive branches are completely dominated by O atoms above the gap (see the partial density of state, DOS, in Supplementary Fig. 3), which has almost equal group velocities of BiCuSeO and BiAgSeO (Supplementary Fig. 4). One of the differences is the slighter softening of acoustic phonons in BiAgSeO, especially the transverse mode along Γ–M (diagonal direction of the ab plane), showing a large drop at the M-point compared to other modes. Such acoustic phonon softening will drive extremely low group velocity and thus softer mechanical properties in BiAgSeO. Table 1 lists the mechanical properties in terms of the acoustic phonon group velocity around Γ-point[28] between BiCuSeO and BiAgSeO. The results of BiCuSeO are in good agreement with previous work[29]. It is found that all of the elastic constants and modulus are lower in BiAgSeO, which is well predicted by our conventional cognition. The second difference is the phonons in the normalized energy range of 0.1–0.4 (~ 5–20 meV in the exact energy range in Supplementary Fig. 3). The branches in BiCuSeO almost form two flat bands (one is around 10 meV, the other is around 20 meV), indicating that the group velocities in this region are actually lower in BiCuSeO

(Supplementary Fig. 4). Thus, phonons below the gap are responsible for the difference in thermal conductivity between these two systems.

Excluding the influence of group velocity, the relaxation time was calculated (Fig. 1d). Below the gap, the relaxation time of BiCuSeO shows two large drops, which are closely related to the two flat bands in the phonon dispersion. Above the gap, there is still a relatively large drop in BiCuSeO, indicating that the heat-carried highly dispersive phonons are strongly scattered. Based on the perturbation theory to first-order in terms of the third-order IFCs, the relaxation time (τ) is determined by two terms: the third-order interatomic potentials (scattering strength) and the scattering phase space (available scattering channels)[30,31].

First, we sorted the representative third-order IFCs from all the triplets (Supplementary Fig. 5) to estimate the scattering strength (Fig. 2a). It can be seen that the IFC of most triplets is comparable in both systems. The only exception is CuCuCu, which has a larger IFC of 1.6 times than the value of AgAgAg, indicating that the difference in anharmonicity is due to the different roles of Cu and Ag in vibration. Second, the phonon scattering space was sorted into four groups, namely the aaa, aao, aoo, and ooo groups, which represent the a (acoustic) $+ a \to a$, $a + a \to o$ (optical), $a + o \to o$, and $o + o \to o$ processes, respectively (Fig. 2b). aoo and ooo groups provide more scattering channels in both systems. aoo group is less in BiCuSeO than in BiAgSeO, while ooo group is the

Table 1. Comparison of elastic properties between BiCuSeO and BiAgSeO.

	C_{11}	C_{33}	C_{44}	C_{66}	C_{12}	C_{13}	B	G	E
BiCuSeO	152.69	100.91	38.71	45.49	70.21	61.91	88.26	38.73	101.36
BiAgSeO	124.96	92.11	21.95	45.51	64.30	46.83	73.11	30.16	76.63

The unit of elastic constants (C_{ij}) and Young's moduli (E) is GPa, and that of bulk moduli (B) and shear moduli (G) is GPa^{-1}.
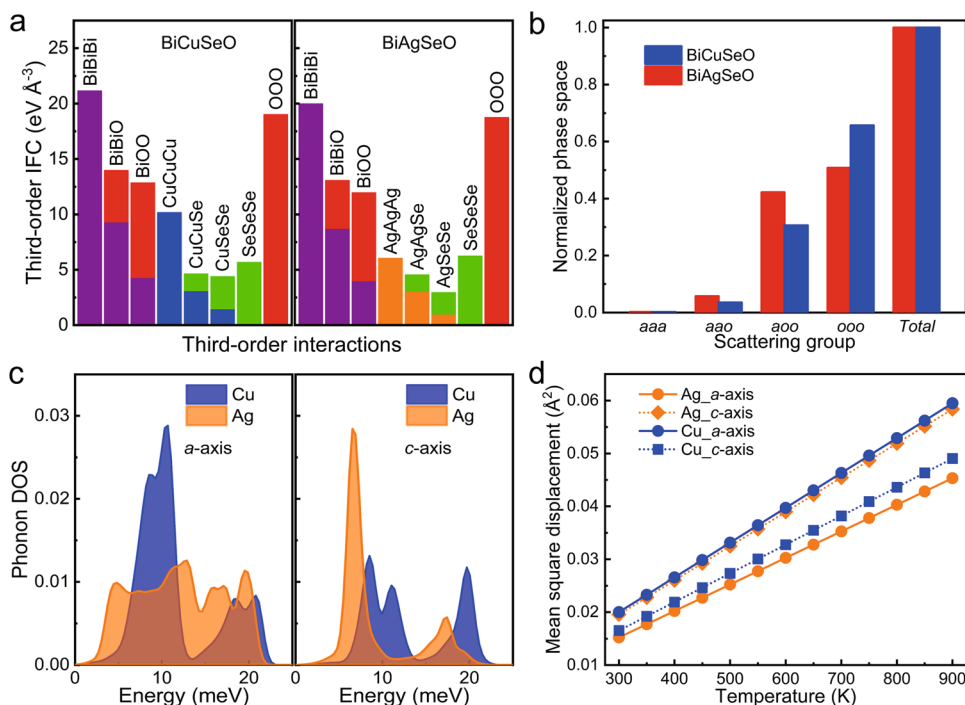

Fig. 2 Atomic vibration analysis for the relaxation time in BiCuSeO and BiAgSeO. a Third-order interatomic force constants (IFCs) of the representative interactions in BiCuSeO (left panel) and BiAgSeO (right panel). **b** Normalized phase space for phonon scattering channels. a and o stand for the acoustic and optical phonons, respectively. **c** Phonon density of state (DOS) of Cu and Ag along the a- (left panel) and c-axes (right panel). **d** Mean square displacement of Cu and Ag along the a- and c-axes.

opposite. As discussed above, the O dominated optical phonons have a significant contribution to thermal conductivity. Thus, the more *ooo* group in BiCuSeO will enable more scattering of these phonons, which is attributed mostly to the two flat optical bands based on the selection rule.

From the partial phonon DOS in Supplementary Fig. 3, it is found that the two flat bands, corresponding to the two phonon peaks, are mainly dominated by Cu/Ag and Se, although the DOS of Ag and Se are more discrete in BiAgSeO. Thus, the thermal conductivity anomaly can be further traced to the vibration of Cu/Ag in the CuSe$_4$/AgSe$_4$ tetrahedron. Figure 2c shows the anisotropic phonon DOS of Cu and Ag. Interestingly, Cu exhibits a sharp peak along the *a*-axis while Ag is along the *c*-axis. This difference in vibrational direction indicates that Cu prefers the in-plane vibration, while Ag tends to vibrate along the out-of-plane direction. In general, the sharp peak in the phonon DOS implies flat dispersion with large atomic displacement (Supplementary Fig. 6). As expected, the calculated mean square displacement (MSD) of Cu exactly exhibits larger values along the *a*-axis than along the *c*-axis with an anisotropy ratio of ~1.2 over the temperature range, while Ag behaves inversely with an anisotropy ratio of ~0.75. Based on the anisotropic thermal conductivity of BiCuSeO and BiAgSeO, it is revealed that the in-plane rattling-like Cu drives lower thermal conductivity in BiCuSeO.

Local symmetry distortion and chemical bonding

To further confirm the anisotropic vibration of Cu and Ag, the projected electronic band structure and the crystal orbital Hamilton population (COHP) were calculated. Figure 3a, b show the results around the bandgap (three bands each in valence and conduction bands) in BiCuSeO and BiAgSeO, respectively. Details are shown in Supplementary Fig. 7–9. Both systems have an indirect, narrow bandgap, where the energy gap of BiCuSeO (0.56 eV) is a little lower than that of BiAgSeO (0.64 eV). Our

calculation is in moderate agreement with previous predictions[5,8,25] and measurements[20,32]. The conduction band minimum (CBM) is mainly occupied by Bi-6p$_z$ orbital, and the valence band maximum (VBM) is mainly occupied by the hybridization of Se-4p$_y$ and Cu-3d/Ag-4d (d$_{xz}$/d$_{yz}$ in d-t$_{2g}$[33]) orbitals, which is similar as other valence band extremes (VBEs).

Figure 3d draws the diagram of the bonding configuration below the Fermi-level. In the tetrahedrons, it is found that the wavefunction (at VBM and d$_{x2-z2}$-p$_z$ coupling at Γ-point in the third valence band) of Cu and Se is comparable, while that of Ag is less in AgSe$_4$, indicating weaker Ag-Se due to the lower energy of Ag-4d, and thus larger bandgap of BiAgSeO. In Fig. 3c, the strength of the d-p coupling is evaluated by the projected COHP and the integrated value (ICOHP). Both the coupling of Cu-Se and Ag-Se show antibonding behavior, and it is relatively weak of Ag-Se, leading to different electrical properties around the VBM and VBEs energy region (low concentration, discuss later in Fig. 5). COHP with deep levels are also shown in Supplementary Fig. 10. The value of Bi-O is comparable in both systems, while Ag-Se shows a slightly weaker value compared to Cu-Se. This result indicates that Cu/Ag has the largest MSD, followed by Se, Bi, and O.

Furthermore, it is found that the 4d-orbital splitting of Ag is stronger due to the distortion based on the Jahn-Teller effect[34,35], which is reflected by the projected band structure and partial DOS (Supplementary Figs. 7b–9). The bond length of Ag-Se is moderately larger than that of Cu-Se, and the bond angles indicate the large distortion from the regular tetrahedron (Fig. 4a, b). In CuSe$_4$ and AgSe$_4$, two three-center interactions are presented: one is Se1-Cu-Se1 (Se1-Ag-Se1), equivalent to Se2-Cu-Se2 (Se2-Ag-Se2), with $\alpha = 102.47°$ (92.07°), the other is Se1-Cu-Se2 (Se1-Ag-Se2) with $\beta = 113.08°$ (118.81°). In order to understand the difference, the crystal orbital bond index (COBI) was calculated, which is proposed effectively in quantifying the three-center (atoms) interactions[36]. For two-center interactions, the
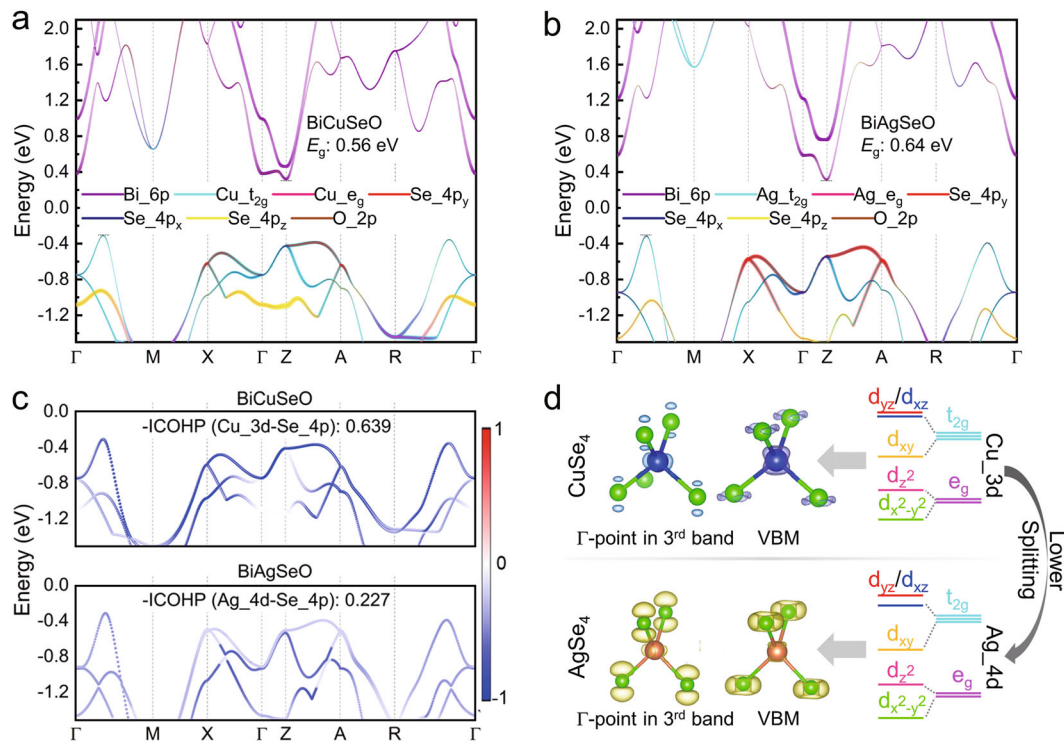

Fig. 3 Electronic band structure and chemical bonding in BiCuSeO and BiAgSeO. (**a**, **b**) are the projected band structure of BiCuSeO and BiAgSeO, respectively. **c** Projected crystal orbital Hamilton population (COHP) of the d-p coupling of Cu/Ag-Se. Color bar indicates antibonding (−1), nonbonding (0), and bonding (1). **d** Diagram of the energy level of Cu-3d and Ag-4d orbitals in three valence bands. Blue, orange, and green balls indicate the Cu, Ag, and Se atoms. Wavefunctions are shown around the atoms.
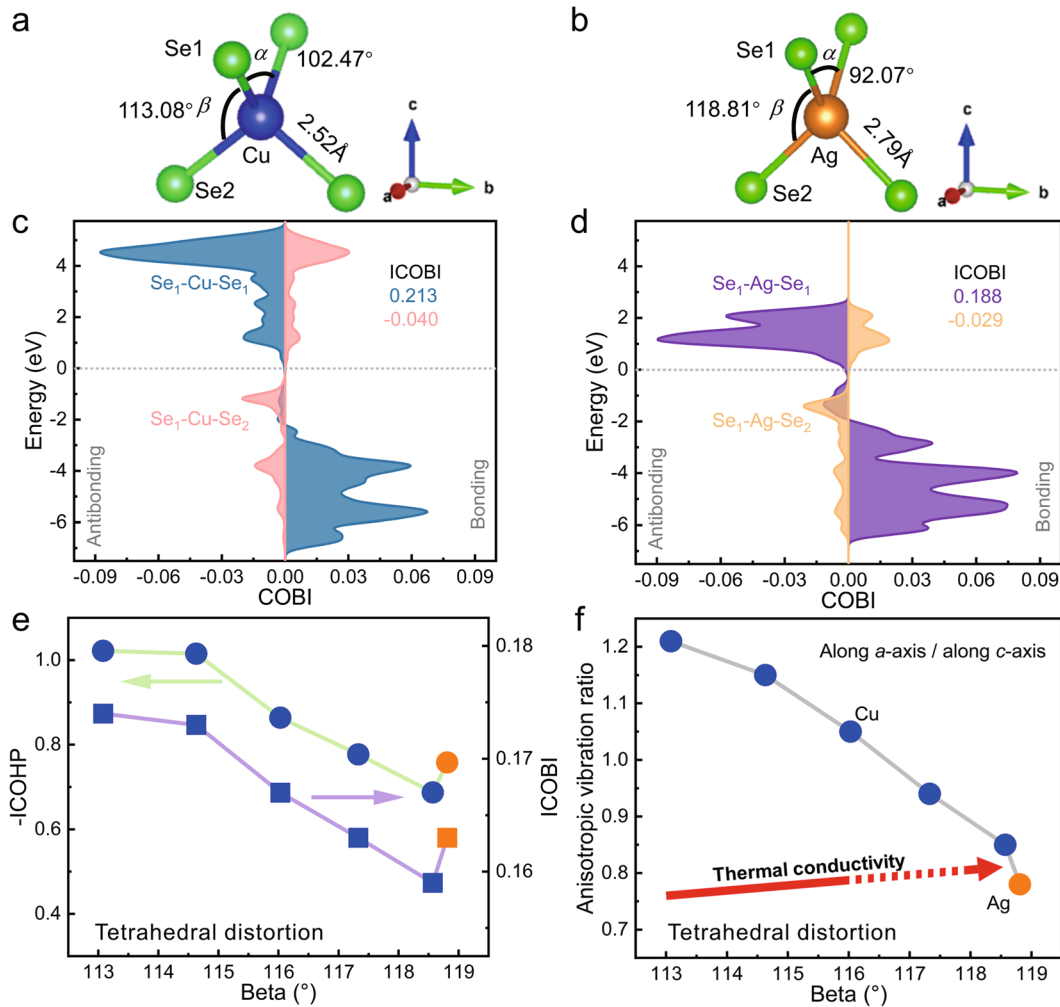
Fig. 4 Local structure distortion induced the anisotropic vibration in BiCuSeO and BiAgSeO. (**a**, **b**) are the local structure of $CuSe_4$ and $AgSe_4$ tetrahedrons, respectively. (**c**, **d**) are the three-center interactions evaluated by the crystal orbital bond index (COBI) and the integrated value (ICOBI) of $CuSe_4$ and $AgSe_4$ tetrahedrons, respectively. **e** Integrated crystal orbital Hamilton population (ICOHP) and ICOBI of evolved $CuSe_4$. **f** Anisotropic vibration ratio of the mean square displacement of Cu along the a- and c-axes.

integrated COBI (ICOBI) is inconsistent with the result of COHP (Supplementary Fig. 11). For three-center interactions, Se1-Cu-Se1 (Se1-Ag-Se1) is significantly larger than Se1-Cu-Se2 (Se1-Ag-Se2), indicating that the smaller angel between the centers increases the interaction strength (Fig. 4c, d).

The difference in ICOBI between Se1-Cu-Se1 and Se1-Ag-Se1 is responsible for the anisotropic vibration of Cu and Ag. Thus, we modified four distortions of $CuSe_4$ by changing the site of Se along the c-axis, where β (a) evolutes from 113.08° (102.47°) to 118.57° (92.49°), and the bond length (L) is stretched from 2.52 to 2.75 Å. Figure 4e shows that the bond strength of Cu-Se decreases with the increasing β from both the results of -ICOHP and ICOBI, approaching the value of Ag-Se. In Supplementary Fig. 12, it is found that the ICOBI of Se1-Cu-Se1 is slightly decreased with the small angle evolution, while that of Se1-Cu-Se2 is basically unchanged, indicating that the three-center interactions along the c-axis are suppressed. The phonon dispersions around the flat band region of the original one become dispersive, especially the modes (like the flexure mode[37]) at the M- and A-point, showing a similar drop as those in BiAgSeO, although they are unstable in larger distorted structures with β (L) = 117.33° (2.69 Å) and 118.57° (2.75 Å). The phonon DOS of Cu along the c-axis (a-axis) becomes more localized (delocalized) with the evolution of local structure, indicating that the vibrational direction of Cu is rotated and holds

a tendency along c-axis like Ag, as also confirmed by the decreased anisotropic ratio in Fig. 4f. Supplementary Fig. 13 shows the anisotropic thermal conductivity of the stable distorted structure with β (L) = 116.03° (2.63 Å). As expected, the average thermal conductivity is exactly enhanced because κ_a is enhanced and κ_c is reduced compared to the original structure.

Electrical transport properties

The difference in electrical transport properties between BiCuSeO and BiAgSeO is also briefly investigated based on the local structure distortion. Figure 5 shows the temperature-dependent electrical conductivity, Seebeck coefficient, power factor (PF), and figure of merit as a function of carrier concentration in a p-type system, and the anisotropic results are shown in Supplementary Fig. 14 for comparison. The electrical conductivity shows high anisotropy, while the Seebeck shows relatively high isotropy, which agree well with previous measurements[38]. Here, the constant electron–phonon coupling approximation is used to overcome the limitation of the constant RTA method in evaluating the electrical conductivity[39], as shown in Supplementary Fig. 15a. Since there is no experimental report on the electrical transport of BiAgSeO so far, we only compared the calculation with the previous experiment of BiCuSeO (Supplementary Fig. 15b, c). With the concentration level at 10^{18} (pristine system) and 5×10^{21} cm^{-3}
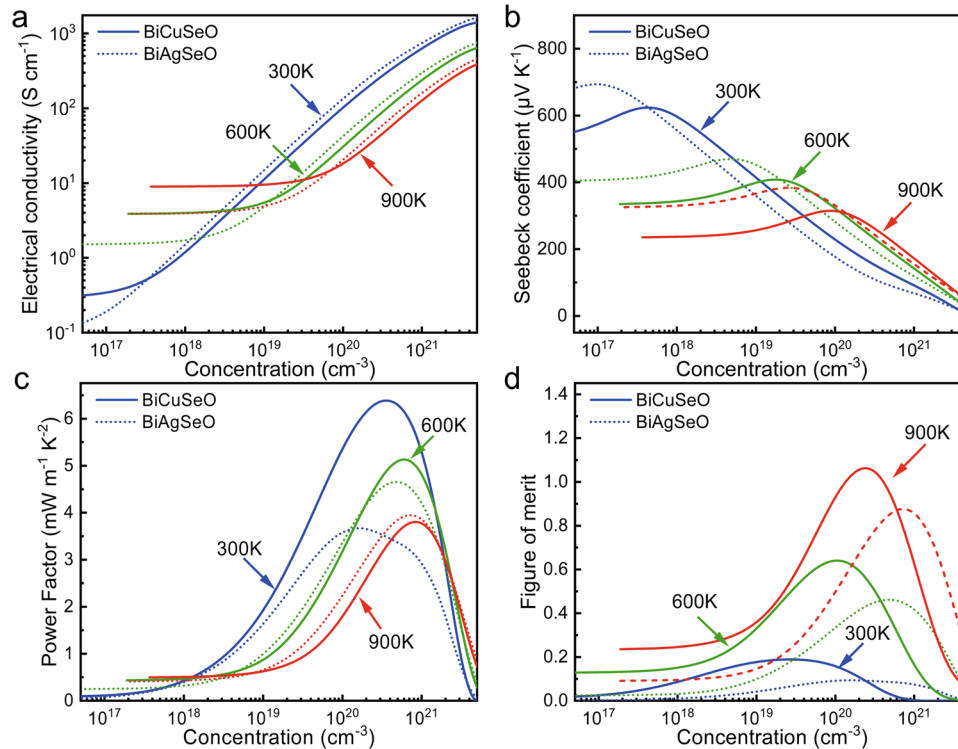
Fig. 5 Temperature-dependent properties of BiCuSeO and BiAgSeO. a Electrical conductivity. **b** Seebeck coefficient. **c** Power factor. **d** Figure of merit.

(doped system)[14], our calculation shows good agreement with the experiment[14] except for the Seebeck coefficient at 10^{18} cm^{-3}. As reported, BiCuSeO exhibits a semiconducting behavior at low concentrations, while it changes to a metal-like behavior at high concentrations. Such behavior is well reproduced by our calculation. In general, the trend of electrical conductivity with temperature is opposite to that of the Seebeck coefficient based on the transport coefficients equations[40], and our calculation agrees well with previous calculations[8,25].

Moreover, it is found that in high concentrations, the electrical conductivity of BiAgSeO is larger than that of BiCuSeO, while the results are opposite in low concentrations. Since the calculation is based on the electronic structure, such behavior is mainly attributed to the effective mass. In the high concentrations (from VBM to deep energy levels), BiAgSeO shows more highly dispersive bands due to the lower energy and greater splitting of the Ag-4d orbital. The calculated hole effective mass of BiAgSeO ($-0.173m_e$ around the VBM and $-0.534m_e$ around the VBE at Z-point) is slightly lower than that of BiCuSeO ($-0.224m_e$ around the VBM and $-0.617m_e$ around the VBE at Z-point). Considering the lower relaxation time (Supplementary Figure 15a), the electrical conductivity is higher, and the Seebeck coefficient is lower in BiAgSeO than in BiCuSeO. However, in low concentrations (below 2.5×10^{17}, 2×10^{19}, and 1×10^{20} cm^{-3} at 300, 600, and 900 K, respectively), where the energy levels are slightly higher than the VBM and VBEs, the electrical conductivity and Seebeck coefficient show the opposite behavior to those in high concentrations. Such behavior might be attributed to the weaker d-p coupling and larger bandgap in BiAgSeO. Overall, PF shows strong temperature dependence. At 300 K, BiCuSeO exhibits higher values over the concentration range, while above 600 K, BiCuSeO and BiAgSeO have comparable values with a competitive mechanism over the concentration range. By considering only the lattice thermal conductivity, we obtained ZT with a rough value, which indicates that BiCuSeO may have better thermoelectric performance for the mid-temperature application (Fig. 5d and Supplementary Fig. 15d).

In conclusion, the abnormal thermal conduction in layered BiCuSeO and BiAgSeO has been explained by solving the Boltzmann thermal equation based on first-principles calculations. The main difference between these two materials is the local structure distortion of CuSe$_4$ and AgSe$_4$ tetrahedrons. The smaller distorted CuSe$_4$ offers larger third-order interatomic force constants and in-plane displacement for Cu, resulting in two flat bands (localized peaks) in the phonon dispersion (DOS). This phonon behavior holds ultralow group velocities and strongly scatters the highly dispersive phonons dominated by the Bi-O layer through the abundant aoo and ooo scattering channels, thus lowering the thermal conductivity in BiCuSeO. These results reveal the microscopic mechanism of ultralow thermal conductivity by linking the ions, bonding, hetero-layers, and transport properties, provide new insights for probing the anomalous thermal conductivity in similar systems, and offer a reference for tuning thermoelectric performance in related materials as well. Based on the conclusion above, following issues are also proposed and might be further considered by interested researchers:

(1) As the polyhedral distortion has significant impact on the transport, it will be powerful to improve the thermoelectric performance by tuning the distortion degree using state-of-the-art synthesis techniques, such as high pressure.

(2) As about 30% of the heat-carrying optical phonons are dominated by oxygen, it is better to suppress the dispersiveness of oxygen-dominated phonons, which will reduce the average phonon group velocity. One proposed method is to weaken the bonds of oxides through chemical control.

METHODS

First-principles calculations

First-principles calculations are performed in the projector-augmented wave (PAW) framework as implemented in the Vienna Ab Initio Simulation Package (VASP) and DS-PAW software[41-43].

Generalized gradient approximation of Perdew-Burke-Ernzerhof for the exchange-correlation functional was used, and optPBE functional[44] was also used to evaluate the interlayer force for layered BiCuSeO and BiAgSeO. Energy cut-off of 600 eV was set for the plane-wave basis based on the maximum energy of the atom in the potential. Brillouin zone of the reciprocal space was sampled as $6 \times 6 \times 3$ based on the convergence test (Supplementary Fig. 16a). The force components of each atom are smaller than 0.0001 eV/Å, and the difference of total energy is smaller than 10^{-8} eV. The lattice constants were fully relaxed for both the two systems and in good consistent with the experiment[7,20], where $a = b = 3.937$ Å and $c = 8.958$ Å for BiCuSeO, and $a = b = 4.018$ Å and $c = 9.480$ Å for BiAgSeO. Balancing the computational cost and accuracy, the electronic transport properties were implemented in the TransOpt code[39] by using the Boltzmann transport theory. Electronic group velocity through the momentum matrix method. The relaxation time is calculated by deformation potential method and the constant electron-phonon coupling approximation.

Second-order IFCs were calculated by the finite difference method with a $3 \times 3 \times 2$ supercell in Phonopy code[45] due to the existing imaginary part in the $2 \times 2 \times 1$ and $2 \times 2 \times 2$ supercells (Supplementary Fig. 16b–d). The Brillouin zone of the reciprocal space for the supercell calculation was sampled as $4 \times 4 \times 3$, which is well sufficient based on the above sample for the primitive cell calculation. Third-order IFCs were also calculated with a $3 \times 3 \times 2$ supercell by considering the eight-nearest neighbor interactions to capture the basic phonon scattering processes embedded in ShengBTE package[46], and the phonon transport properties were obtained by solving the phonon Boltzmann transport equation. More detailed calculation for electrical and thermal transport properties can be found in Supplementary Notes.

DATA AVAILABILITY

The data supporting the findings of this study are available within this article and its Supplementary Information. Additional data are available from the corresponding author on reasonable request.

REFERENCES

1. He, J. & Tritt, T. M. Advances in thermoelectric materials research: Looking back and moving forward. *Science* **357**, eaak9997 (2017).
2. Ren, G.-K. et al. Layered oxygen-containing thermoelectric materials: Mechanisms, strategies, and beyond. *Mater. Today* **29**, 68–85 (2019).
3. Zheng, J., Wang, D. & Zhao, L.-D. An update review on n-type layered oxyselenide thermoelectric materials. *Materials* **14**, 3905 (2021).
4. Yang, Y. et al. Seeking new layered oxyselenides with promising thermoelectric performance. *Adv. Funct. Mater.* **32**, 22146 (2022).
5. Wang, N. et al. Band degeneracy enhanced thermoelectric performance in layered oxyselenides by first-principles calculations. *npj Comput. Mater.* **7**, 18 (2021).
6. Gibson, Q. D. et al. Low thermal conductivity in a modular inorganic material with bonding anisotropy and mismatch. *Science* **373**, 1017–1022 (2021).
7. Zhao, L.-D. et al. BiCuSeO oxyselenides: new promising thermoelectric materials. *Energy Environ. Sci.* **7**, 2900–2924 (2014).
8. Zou, D., Xie, S., Liu, Y., Lin, J. & Li, J. Electronic structures and thermoelectric properties of layered BiCuOCh oxychalcogenides (Ch = S, Se and Te): First-principles calculations. *J. Mater. Chem. A* **1**, 8888 (2013).
9. Zhu, H. et al. High pressure synthesis, structure and thermoelectric properties of BiCuChO (Ch = S, Se, Te). *J. Eur. Ceram. Soc.* **37**, 1541–1546 (2017).
10. Natarajan, A. R. et al. High thermoelectric performance of layered LaAgXO (X=Se,Te) from electrical and thermal transport calculations. *Phys. Rev. Mater.* **7**, 025405 (2023).
11. Tippireddy, S., Prem Kumar, D. S., Das, S. & Mallik, R. C. Oxychalcogenides as thermoelectric materials: An overview. *ACS Appl. Energy Mater.* **4**, 2022–2040 (2021).
12. Wang, J. et al. Thermoelectric properties of Bi_2O_2Se single crystals. *Appl. Phys. Lett.* **119**, 081901 (2021).
13. Ruleova, P. et al. Thermoelectric properties of Bi_2O_2Se. *Mater. Chem. Phys.* **119**, 299–302 (2010).
14. Li, J. et al. A high thermoelectric figure of merit $ZT > 1$ in Ba heavily doped BiCuSeO oxyselenides. *Energy Environ. Sci.* **5**, 8543 (2012).
15. Feng, D. et al. Investigation into the extremely low thermal conductivity in Ba heavily doped BiCuSeO. *Nano Energy* **27**, 167–174 (2016).
16. Zhao, L. D. et al. $Bi_{1-x}Sr_xCuSeO$ oxyselenides as promising thermoelectric materials. *Appl. Phys. Lett.* **97**, 092118 (2010).
17. Liu, Y. et al. Remarkable Enhancement in Thermoelectric Performance of BiCuSeO by Cu Deficiencies. *J. Am. Chem. Soc.* **133**, 20112–20115 (2011).
18. Li, F. et al. Polycrystalline BiCuSeO oxide as a potential thermoelectric material. *Energy Environ. Sci.* **5**, 7188 (2012).
19. Pei, Y.-L. et al. High thermoelectric performance of oxyselenides: intrinsically low thermal conductivity of Ca-doped BiCuSeO. *NPG Asia Mater.* **5**, e47–e47 (2013).
20. Zhang, C. et al. Low thermal conductivity in heteroanionic materials with layers of homoleptic polyhedra. *J. Am. Chem. Soc.* **144**, 2569–2579 (2022).
21. Schlichting, K. W., Padture, N. P. & Klemens, P. G. Thermal conductivity of dense and porous yttria-stabilized zirconia. *J. Mater. Sci.* **36**, 3003–3010 (2001).
22. Zeier, W. G. et al. Thinking like a chemist: intuition in thermoelectric materials. *Angew. Chem. Int. Ed.* **55**, 6826–6841 (2016).
23. Slack, G. A. Nonmetallic crystals with high thermal conductivity. *J. Phys. Chem. Solids* **34**, 321–335 (1973).
24. Shao, H., Tan, X., Liu, G.-Q., Jiang, J. & Jiang, H. A first-principles study on the phonon transport in layered BiCuOSe. *Sci. Rep.* **6**, 21035 (2016).
25. Fan, D. D. et al. Understanding the electronic and phonon transport properties of a thermoelectric material BiCuSeO: A first-principles study. *Phys. Chem. Chem. Phys.* **19**, 12913–12920 (2017).
26. Li, J. et al. Predicting excellent anisotropic thermoelectric performance of the layered oxychalcogenides BiAgOCh (Ch=S, Se, and Te). *Comput. Mater. Sci.* **171**, 109273 (2020).
27. Ren, G.-K. et al. Complex electronic structure and compositing effect in high performance thermoelectric BiCuSeO. *Nat. Commun.* **10**, 2814 (2019).
28. Antonangeli, D. et al. Elasticity of Cobalt at High Pressure Studied by Inelastic X-Ray Scattering. *Phys. Rev. Lett.* **93**, 215505 (2004).
29. Saha, S. K. & Dutta, G. Elastic and thermal properties of the layered thermoelectrics BiOCuSe and LaOCuSe. *Phys. Rev. B* **94**, 125209 (2016).
30. Cowley, R. A. Anharmonic crystals. *Rep. Prog. Phys.* **31**, 123–166 (1968).
31. Wei, B. et al. Matryoshka phonon twinning in α-GaN. *Commun. Phys.* **4**, 227 (2021).
32. Hiramatsu, H. et al. Crystal structures, optoelectronic properties, and electronic structures of layered oxychalcogenides MCuOCh (M = Bi, La, Ch = S, Se, Te): Effects of electronic configurations of M3+ ions. *Cheminform* **39**, 326–334 (2008).
33. Lucovsky, G. Electronic structure, amorphous morphology and thermal stability of transition metal oxide and chalcogenide alloys. *J. Optoelectron. Adv. M.* **3**, 155–166 (2001).
34. Kugel', K. I. & Khomskiĭ, D. I. The Jahn-Teller effect and magnetism: transition metal compounds. *Sov. Phys. Usp.* **25**, 231 (1982).
35. Muhammady, S. et al. Unrevealed electronic and optical properties of the layered oxychalcogenides (LaO)CuCh(Ch=S, Se, Te): A density-functional study. *Jpn. J. Appl. Phys.* **56**, 121201 (2017).
36. Müller, P. C., Ertural, C., Hempelmann, J. & Dronskowski, R. Crystal orbital bond index: Covalent bond orders in solids. *J. Phys. Chem. C* **125**, 7959–7970 (2021).
37. Cai, Q., Wei, B., Sun, Q., Said, A. H. & Li, C. Monolayer-like lattice dynamics in bulk WSe_2. *Mater. Today Phys.* **28**, 100856–100856 (2022).
38. Sui, J. et al. Texturation boosts the thermoelectric performance of BiCuSeO oxyselenides. *Energy Environ. Sci.* **6**, 2916 (2013).
39. Li, X. et al. TransOpt. A code to solve electrical transport properties of semiconductors in constant electron–phonon coupling approximation. *Comput. Mater. Sci.* **186**, 110074–110074 (2021).
40. Yang, J. et al. On the tuning of electrical and thermal transport in thermoelectrics: an integrated theory–experiment perspective. *NPJ Comput. Mater.* **2**, 15015 (2016).
41. Blöchl, P. E. Projector augmented-wave method. *Phys. Rev.* **50**, 17953–17979 (1994).
42. Kresse, G. & Furthmuller, J. Efficiency of ab-initio total energy calculations for metals and semiconductors using a plane-wave basis set. *Comput. Mater. Sci.* **6**, 15–50 (1996).
43. Kresse, G. & Furthmuller, J. Efficient iterative schemes for ab initio total-energy calculations using a plane-wave basis set. *Phys. Rev. B* **54**, 11169–11186 (1996).
44. Klimes, J., Bowler, D. R. & Michaelides, A. Chemical accuracy for the van der Waals density functional. *J. Phys. Condens. Matter* **22**, 022201 (2009).
45. Togo, A. & Tanaka, I. First principles phonon calculations in materials science. *Scr. Mater.* **108**, 1–5 (2015).

46. Wu, L., Carrete, J., Katcho, N. A. & Mingo, N. Shengbte: A solver of the Boltzmann transport equation for phonons. *Comput. Phys. Commun.* **185**, 1747–1758 (2014).

AUTHOR CONTRIBUTIONS

B.W. and Y.-H.L. conceived the idea. B.W. and J.L. conducted the simulation. B.W., Y.Y., W.L., Z.Z., Y.Z., and W.Z. conducted the analysis and discussion. Y.C. and S.L. provided advices on this work. C.-W.N. and Y.L. supervised the manuscript. All authors contributed to the writing and review of the manuscript.

COMPETING INTERESTS

The authors declare no competing interests.

ADDITIONAL INFORMATION

Supplementary information The online version contains supplementary material available at https://doi.org/10.1038/s41524-023-01097-2.

Correspondence and requests for materials should be addressed to Yuan-Hua Lin.

Reprints and permission information is available at http://www.nature.com/reprints

Publisher's note Springer Nature remains neutral with regard to jurisdictional claims in published maps and institutional affiliations.